ICAS 2020 SHANGHAI
International Council of the Aeronautical Sciences
32nd Congress of the International Council of the Aeronautical Sciences
September 6-10, 2021
Pudong Shangri-La, Shanghai, China

AERODYNAMIC AND STRUCTURAL MODELING IN THE ROTORCRAFT MULTI-PHYSICS SIMULATION VAST

Johannes Hofmann[1], Maximilian Mindt[1] & Felix Weiss[1]

[1]German Aerospace Center (DLR) - Institute of Flight Systems

Abstract

Comprehensive aeromechanics simulation for rotorcraft is a complex field involving models from different disciplines with very different structure and complexity. VAST (*Versatile Aeromechanics Simulation Tool*) addresses this field with a new approach involving a generic coupling of state-space models. The paper describes the approach and focuses on aerodynamic and structural methods used in the framework. The implemented models for aerodynamics include unsteady aerodynamics based on a semi-empirical analytical model for the blade sectional airloads and a vortex-lattice model for the computation of the rotor wake. The structural modeling is based on a generic multi-body approach.

Keywords: multi-physics simulation, helicopter, fast aerodynamics, multi-body

1. Introduction

Comprehensive aeromechanics codes are a very important engineering tool for helicopter design and phenomenological investigations. The nature of the helicopter problem leads to a very tight coupling between disciplines, necessitating fast tools encompassing structure, dynamics, aerodynamics and more. These codes are called comprehensive simulation codes. To make use of advances in software technology and to integrate several in-house models the Institute of Flight Systems (FT) of the German Aerospace Center (DLR) together with the Institute for Software Technology are developing a new framework for low and medium fidelity simulation of rotary wing aircraft. Among other areas of application the *Versatile Aeromechanics Simulation Tool* (VAST) is being developed to act as a computational backbone of an integrated rotorcraft design and optimization chain.

The principal idea is a coupled system of models that are expressed as state-space models (see fig. 2a) with the implicit system of coupling equations being automatically resolved. This approach allows generic methods for solving the system to be developed unlike many other codes in the field which require highly specialized solution procedures and are thus rigid to change. The logic for the model interconnection is kept completely outside of the simulation process and computed as a pre-step. The basis of physical models is taken from existing research codes like the in-house rotor simulation S4 and the FT-Freewake [1] as well as implementation of proven numerical models like a dynamic wake model [2] and its recent extensions. The structural dynamics is calculated using an internal structural model using rigid multi-body dynamics as well as an adaptive coupling to SIMPACK [3]. The first version of the code has been developed in the frame of the DLR project VicToria. The development is now being continued in a number of internally and externally funded projects.

The first chapter of this paper gives an overview of the generic coupling approach for the single models and the encompassing framework in VAST. The subsequent chapters focus on the most important model groups in the context of helicopter simulation, namely aerodynamics and structural dynamics. Verification of the implemented functionality is shown in the respective chapters as well.

2. The VAST Framework

The simulation framework can be divided in four parts as shown in fig. 1). The *initialization* module handles the configuration of the system to be simulated, reads all input data and provides all parts of

the framework with parameters needed for execution. The *core* performs a non-linear time simulation for the specified models and simulation parameters. Additionally, the *system analysis* component contains all methods of analysis that either use the non-linear time simulation (e. g. trim) or operate on the models directly (e. g. eigen-analysis). Overall, the *process control* module essentially executes a list of tasks for the calculation (e.g. initialize the system → perform a trim → perform a time simulation with given inputs → etc.).

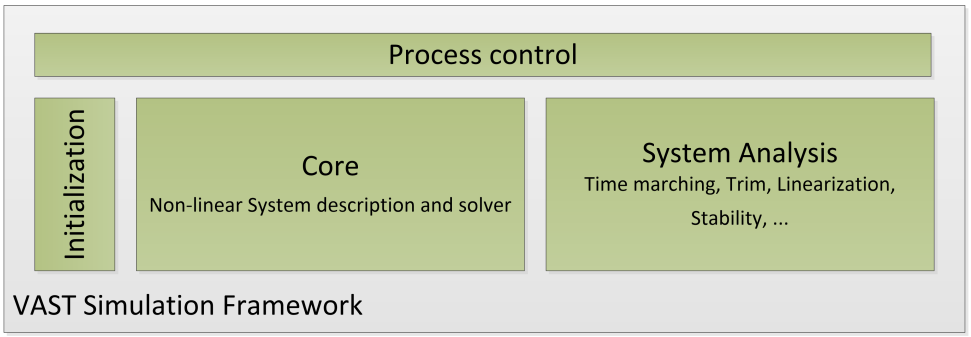

Figure 1 – VAST simulation framework

What sets VAST apart from other helicopter simulation software is its generic approach, which will be described in more detail in the following sections. In principle, it is nowhere explicitly assumed that the user does actually want to simulate a helicopter. Instead, a very general model concept that is described in section 2.1 is used and coupling of these models is performed by a solver that is in no way specific, as shown in section 2.2. Still, the generic approach allows to implement helicopter-specific aspects as a particular model. Therefore, the VAST architecture successfully strikes a balance between generality and being tailored to the specific application.
The VAST *core* includes all parts of the code that are needed to perform a time simulation of the configured dynamic system. It consists of an arbitrary number of state-space models with inputs and outputs, which are coupled to each other by a solver for the resulting differential-algebraic equations.

2.1 Generic State-Space Models

The basis of the VAST *core* component is an arbitrary number of models, each one being of the form depicted in fig. 2a.
For every model i, it is assumed that its dynamic behavior can be described by a number of states, collected in a time-varying vector $\mathbf{x}_i(t)$. Furthermore, it is assumed that the dynamics may depend on a number of inputs $\mathbf{u}_i(t)$ and that a model may provide additional outputs $\mathbf{y}_i(t)$, which can be computed from the states and inputs. All in all, the dynamics shall be governed by the ordinary differential equation with inputs and outputs

$$\dot{\mathbf{x}}_i = \mathbf{f}_i(\mathbf{u}_i, \mathbf{x}_i, t), \tag{1a}$$

$$\mathbf{y}_i = \mathbf{g}_i(\mathbf{u}_i, \mathbf{x}_i, t) \tag{1b}$$

where, for simplicity, the time-dependency of $\mathbf{x}_i, \mathbf{y}_i, \mathbf{u}_i$ have been omitted. The functions $\mathbf{f}$ and $\mathbf{g}$ in (1) describe the dependence of the states' rate of change and the outputs, respectively, on the states and the inputs. Since it is assumed that the dynamic system is described entirely by (1), these two functions are the main functionality that needs to be implemented for such a generic state-space model to be able to use it in VAST.
Additionally, some minor infrastructural functionality needs to be provided, which can also be seen in fig. 2a. Most importantly, a *model factory* needs to be provided, which reads in a certain XML node of the configuration file and initializes the model with the specified model parameters. Moreover, some additional functionality may be provided, such as a manually implemented gradient of the output variables with respect to the input variables, which will otherwise be computed by numerical differentiation if needed by the solver.
It is important to notice that the different models in a configuration do not have any knowledge about each other. Each of them is a distinct and independent piece of software, which is only connected

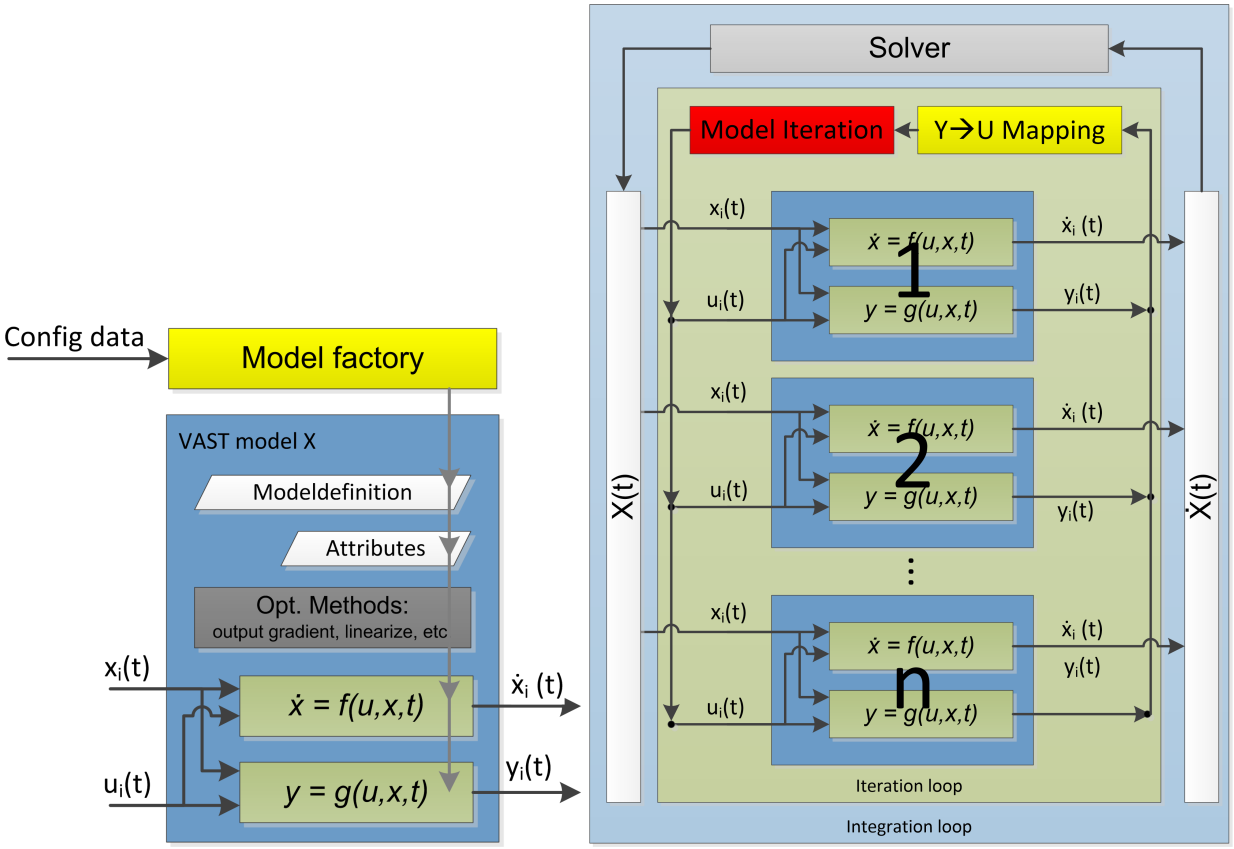

(a) Generic state-space model (b) The VAST solver

Figure 2 – Generic state-space model and the VAST solver

to the solver, but not directly to the other models. The VAST *core* and the solver do not make any assumptions about the models apart from the very generic ones mentioned above. In principle, models can still exchange arbitrary quantities via their inputs and outputs, which makes it possible to use the model framework for a diversity of applications. Moreover, this approach reduces the number of dependencies between different components, which is a clear advantage of VAST, since it is more maintainable and extendable than a software with specific model interdependencies.

2.2 Half-Explicit Time Integration

The general solution strategy of the VAST solver is depicted in fig. 2b. As mentioned above, every model, enumerated with $i = 1, \ldots, n$ in the figure, has a certain number of inputs and outputs, denoted by $\mathbf{u}_i$ and $\mathbf{y}_i$, respectively. Since every input of a model must correspond to the output of another model, for the overall system there is actually only one global vector of outputs $\mathbf{y}$, which is used both as input and output for all models. The entire system of equations then reads

$$\dot{\mathbf{x}} = \mathbf{f}(\mathbf{y}, \mathbf{x}, t), \tag{2a}$$

$$\mathbf{y} = \mathbf{g}(\mathbf{y}, \mathbf{x}, t), \tag{2b}$$

where the states of all models are collected in a vector $\mathbf{x}$ respectively. Consequently, the function $\mathbf{f}$ return the time derivative of the states of all models, whereas the function $\mathbf{g}$ computes the outputs of all models. The system in (2) is no longer an ordinary differential equation (like the system in (1)), but is a so-called *differential-algebraic equation (DAE) of index 1*. The equation (2a) is called *differential part*, (2b) is called *algebraic part* of the DAE. A consequence of having at hand a DAE of index 1 is that the algebraic part has a unique solution $\mathbf{y}$ for given $\mathbf{x}$ and t. Moreover, the gradient is locally invertible, which is beneficial for the numerical solution of this equation.

In VAST, the solution of (2) is performed by a *half-explicit time integration scheme*. That is, the differential part (2a) is solved by a standard integrator for ordinary differential equations, whereas

in every time step the algebraic part (2b) is solved by a Newton-like iteration. The latter typically converges in a very small number of iterations, since the respective values from the previous timestep are used as an initial guess, which is already near to the actual solution.
For the coupled DAE system (2), VAST provides two different solvers, an *explicit coupled Runge-Kutta (RK) solver* (see [4]) and an *exponential coupled Runge-Kutta solver*, where the latter has been specifically developed for VAST (see [5]). For both solvers, the respective order can be configured, a standard RK4 solver being the default.

2.3 System Analysis

The VAST software also provides several components for system analysis, the most important being a generic trim component. As it is well-known, the term *trim* describes "the correct adjustment of aircraft controls, attitude, and cargo in order to obtain a desired steady flight condition" [6]. In VAST, the very generic control-theoretic approach from [6] is adopted, where (2) is generalized to obtain

$$\dot{\mathbf{x}}(\mathbf{c}) = \mathbf{f}(\mathbf{y}(\mathbf{c}), \mathbf{x}(\mathbf{c}), \mathbf{c}, t), \tag{3a}$$
$$\mathbf{y}(\mathbf{c}) = \mathbf{g}(\mathbf{y}(\mathbf{c}), \mathbf{x}(\mathbf{c}), \mathbf{c}, t), \tag{3b}$$

where the parameter vector $\mathbf{c}$ denotes all those parameters, which shall be adjusted correctly by the trim method. The vectors $\mathbf{x}(\mathbf{c})$, $\mathbf{y}(\mathbf{c})$ denote the models' states and outputs if the parameters $\mathbf{c}$ are chosen. For a specified vector $\mathbf{c}$, the system in (3) is, therefore, still a DAE of index 1. All trim objectives, that is, the desired steady flight condition, are reformulated as an equation

$$\mathbf{h}(\mathbf{c}) = \mathbf{0}. \tag{4}$$

Here, the function $\mathbf{h}$ may explicitly use the solutions $\mathbf{x}$, $\mathbf{y}$ of (3). For example, for a wind-tunnel trim, where the outputs y_1, y_2, y_3 may represent three force or moment components at the balance a trim objective might be described as

$$\mathbf{h}(\mathbf{c}) = \begin{pmatrix} \mathrm{mean}(y_1(\mathbf{c})) - f_1 \\ \mathrm{mean}(y_2(\mathbf{c})) - f_2 \\ \mathrm{mean}(y_3(\mathbf{c})) - f_3 \end{pmatrix} = \mathbf{0} \tag{5}$$

for a specified desired force $\mathbf{f} = (f_1, f_2, f_3)^{\mathrm{T}}$, where $\mathrm{mean}(\cdot)$ denotes the mean of the corresponding variable over the desired time period. The overall trim problem in VAST is treated by interpreting (4) as a nonlinear least-squares problem, which is then solved by a *Levenberg-Marquardt method* (see [7], section 10.3), an iterative algorithm for such problems. In consequence, in each of the trim iterations, a time integration has to be performed to obtain the values $\mathbf{x}(\mathbf{c})$. The Jacobians that are needed in the *Levenberg-Marquardt method* are computed by numerical differentiation.

3. Aerodynamics

This chapter focuses on the aerodynamic models as fundamental representatives of the interconnected models in the context of helicopter simulation. It is also a demanding model category because of the highly complex flow field around a helicopter. One of the main reasons for this is the flow around the main rotor blades. In forward flight, the rotational speed of the rotor is superimposed with the forward speed. This leads to large variations in flow velocities and angles of attack in the course of every rotation. At the inboard regions of the retreating side, reversed and fully separated flow occurs, while there are trans-sonic flow effects at the tip of the advancing blade. On top of that, high sideward velocities are acting at the airfoils with rapidly changing amplitude and the encountering of the preceding blades' vortices leads to localized drastic changes in angle of attack.
The challenge of a comprehensive simulation tool is to capture all the aerodynamically challenging effects at low computational cost. A method to incorporate the airfoils' response to unsteadiness is to use the response to step changes in the flow conditions – so called indicial functions – and integrate their superposition over time. In VAST, these indicial functions are implemented as developed by Beddoes and Leishman [8] for the noncirculatory response. In contrast to the original model, the circulatory response developed in [8] is only used to calculate the effective flow velocities at the

airfoils. These effective velocities are then fed into an adapted version of the aerodynamic model of Leiss [9]. The benefit of this model is that it can capture the effects of Mach number variation, yawed flow and dynamic stall while retaining an analytical description throughout the whole range of angles of attack. The basic assumption of the model is, that the generation of forces at the blade sections can be replicated by superposition of the contributions of the physical sources. This is shown in fig. 3 for the normal force coefficient C_z, also depicting the variation of the coefficient over normal Mach number Ma_z. The fully separated flow is broken into two contributions, namely that of the noncirculatory detached Newton flow $C_{z,Newton,det}$ and the detached Kirchhoff flow $C_{z,c,det}$. Most important for the unsteady behavior is the attached flow contribution $C_{z,c,att}$, because this yields the so called dynamic stall effect of belated stalling of the airfoil and higher maximum lift generation. More theoretical background for both underlying models and about the merging of these into one unsteady sectional aerodynamic model can be found in [10].

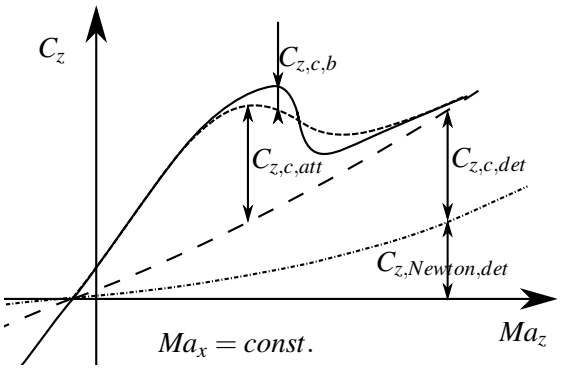

Figure 3 – Distinction of force components by mechanism

The effect of stall overshoot was verified by comparison of VAST calculations to results of computational fluid dynamics (CFD) calculations for a NACA 23012 airfoil with a tabbed trailing edge. The reference results for harmonic oscillations of the airfoil using the DLR CFD code TAU were obtained within the EU-funded project SABRE [11]. The comparison is slightly complicated by the difference in static behavior of the airfoil, which is shown in dashed blue line for the VAST results and in green dash-dot line for the TAU calculations in fig. 4. It can be seen that the steady behavior of the normal force coefficient C_z matches better for positive angles of attack. In the negative angle of attack range, the airfoil already stalls at $-6.5°$ in the TAU calculation, but keeps attached up to an angle of attack of $-13°$ in the VAST model. Because of this discrepancy, the detailed comparison of the results will be focused on the attached flow and stall behavior for positive angles of attack in the following.
Despite the relatively low reduced frequency of $k = 0.05$, large deviations to the static curves of both unsteady VAST as well as TAU calculation can be observed. This is due to the high amplitude of the harmonic oscillation of $20°$. The amplitude of the unstedy changes is not reflected in the reduced frequency, but nevertheless has an influence on the speed of change in flow conditions. Starting to follow the unsteady curves in their pitch up movement at $0°$, the models' results in black as well as the CFD results in red are showing lower values than the corresponding steady curves. This is due to the effective angle of attack at the airfoil being lower than the geometric one since the changes in flow conditions need to be propagated over the airfoil from leading edge to trailing edge. Either this effect is a little stronger in the VAST model or the share of the noncirculatory forces in force generation was more severe in the TAU calculations.
Both calculations show a large impact of dynamic stall. Instead of loss in normal force after the steady stall angle of $9.5°$ (TAU) or $11°$ (VAST), the force coefficient continues to rise up to $16.2°$ (VAST) and even $17°$ (TAU). The maximum values attained are also increased by 47 % in VAST and even 61 % in TAU. The sharper peak and the higher rise of the coefficient in the CFD computation is caused by a discrete vortex that is shed from the blade tip. Vortex shedding is not part of the formulation in VAST. At the turning point of the movement at $20°$, both simulations attain the steady, stalled value shortly, then they continue to drop under the steady values in the nose-down movement of the airfoil. In the later course of the movement, they cross the steady value curves again. This happens when the flow

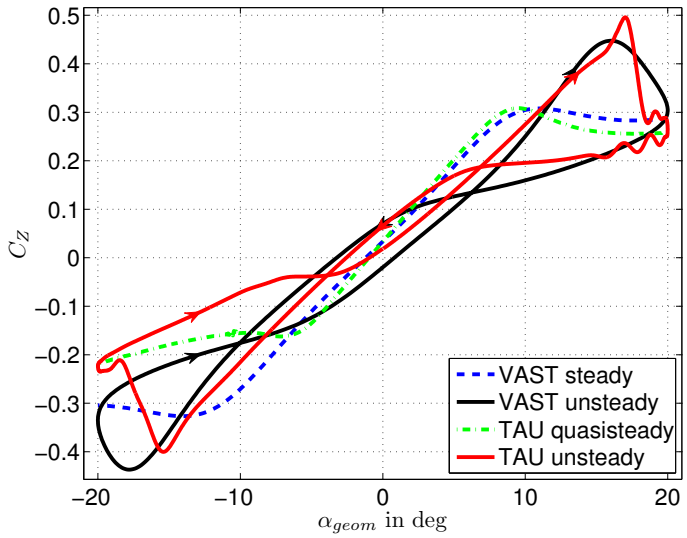

Figure 4 – Normal force coefficient hysteresis for oscillating NACA 23012 airfoil compared to CFD; $Ma = 0.5$, $k = 0.05$, $\Delta\alpha = 20°$

is reattaching to the airfoil and the lag of the effective angle of effect with respect to the geometric angle gets dominant for the unsteady effects once more. In the VAST calculations, this reattachment takes a little longer and the stalled portion of the movement is accompanied by a slightly larger drop in value. Overall, despite some quantitative differences, the shape of the hysteresis and hence the influence of unsteadiness on the normal force coefficient is captured well for this test case. Another test case including a discussion of the moment and tangential coefficients as well can be found in [10].

The downwash of the rotor blades has special importance for helicopters. Because of the blades' circular path, they encounter their own downwash and that of the other blades over and over, leading to a stream tube. Depending on the purpose of the calculation, different fidelity levels are needed for the representation of this phenomenon. If only simple static performance evaluations are to be performed, a static global model as the one developed by Glauert [12] may be sufficient to reproduce the change in the blade section angles of attack. If the development of the inflow, which has a time lag to the change in forces, is relevant, the simple dynamic inflow model proposed by Pitt and Peters [13] and a generalized dynamic wake model [2] can be used in VAST. For the calculation of local blade loads and interaction of aerodynamics and blade dynamics, a Freewake method is available in strongly coupled version in VAST [1]. In this model, the movement of the blade tip vortices and their influence on local flow velocities is traced.

In a validation effort for this Freewake method, the experiments of Caradonna and Tung [14] have been used. This experiment features a model helicopter rotor on a hover test stand and is a standard benchmark for aerodynamic codes. In VAST, the two-bladed rotor was modeled as rigid and with fixed pitch setting. A constant ring area discretization is employed for the 15 aerodynamic elements, i.e., the single elements cover the same ring area over the course of a revolution. The blades are untwisted and have a radius of $R = 1.143\,\mathrm{m}$. In fig. 5, the results of the test case with a pitch $\theta_0 = 8°$ and rotational speed $\Omega = 2250RPM$ leading to a blade tip Mach number of 0.794 are shown.

Via the cut-away of the color-coding in the front half of the wake in fig. 5a, the increase in downward convection of the wake with radius that is only lessened at the tip can clearly be seen. This increase in convection originates in the increase in circulation over radius until the tip loss becomes effective, which is depicted in fig. 5b. An overprediction of the circulation relative to the experimental values in the outboard region up to the influence of the blade tip loss can be identified. In the inboard region, an underprediction is apparent. The calculated overall thrust fits quite well to the experimental data, since both effects roughly cancel each other out.

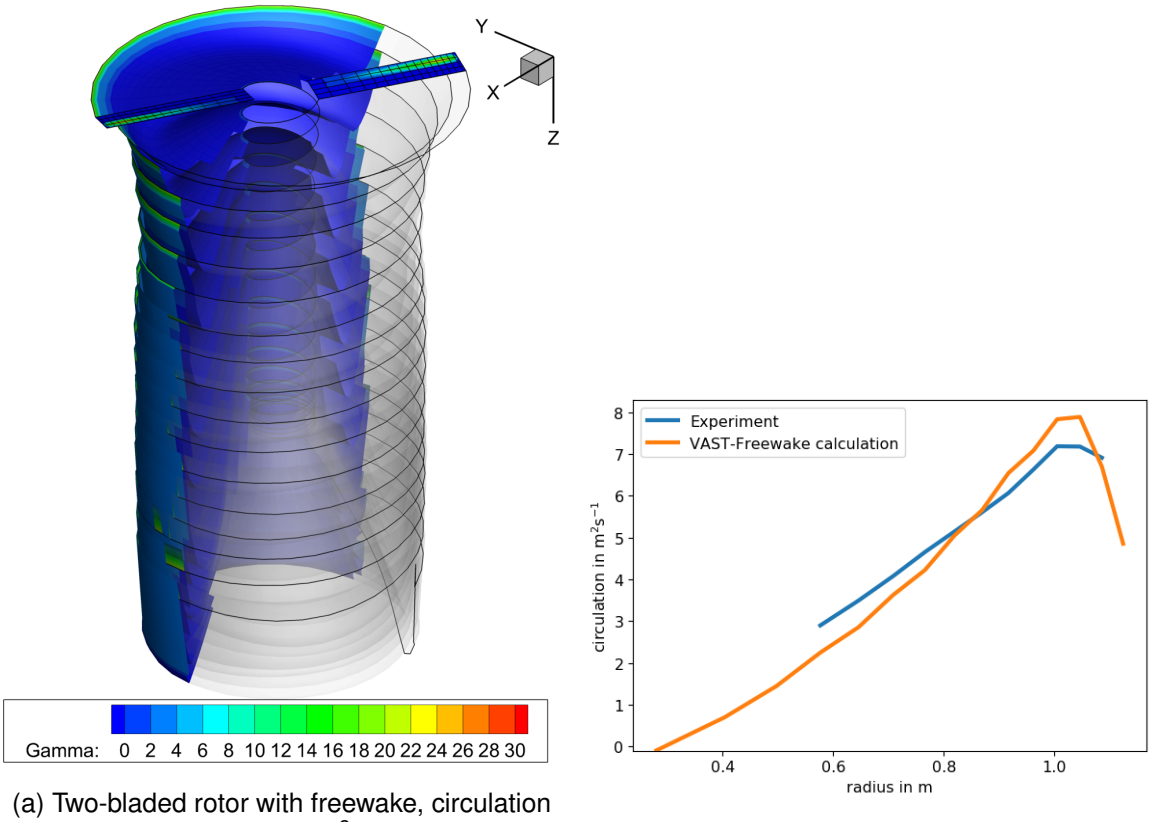

(a) Two-bladed rotor with freewake, circulation Gamma in m^2/s

(b) Circulation distribution over radius

Figure 5 – Freewake test of Caradonna experiment, case with $M_{tip} = 0.794$ and $\theta_0 = 8°$

4. Structural Mechanics

A main characteristic of the system helicopter from the structural point of view is the existence of several parts with large relative motion. Such problems are best described as a multi-body system (MBS). While the rotor or rotors make up only a relatively small part of the total mass, they are subject to large centrifugal forces resulting in a significant impact on the overall system dynamics. Multi-body problems in structural mechanics can be numerically modeled in several ways. In VAST an integrative approach was chosen, modeling the entire structure in one VAST model based on minimal coordinates of the system.

An MBS consists of a multitude of rigid or flexible bodies which are interconnected by joints and affected by internal and external loads. Due to its modular and arbitrary configuration, the MBS in general does not impose any restrictions on the vehicle's architecture. The system's non-linear kinematics is represented exactly. Broad surveys on the considerable amount of MBS research are found in [15] for rigid MBS and in [16] for flexible MBS.

For clarification, fig. 6 depicts an exemplary MBS with the kinematic notation used in the following. Two sets of states and corresponding dynamic equations are distinguished within the MBS: general states within a differential algebraic equation (DAE) and minimal states within an ordinary differential equation (ODE). The subscript I denotes positions or rotational deflections, whereas II indicates translatory or rotational velocities. The superscript i denotes the specific body or joint i. Variables without this index refer to the whole MBS. The body on the right is a general flexible body which can be modeled by superimposing the flexible deformation on the rigid body motion e.g. as described in [16].

4.1 MBS Dynamics Using Minimal States

The dynamic differential equations are originally given in general states z as

$$\mathbf{M}\dot{z} = h + \mathbf{G}^T \lambda, \tag{6}$$

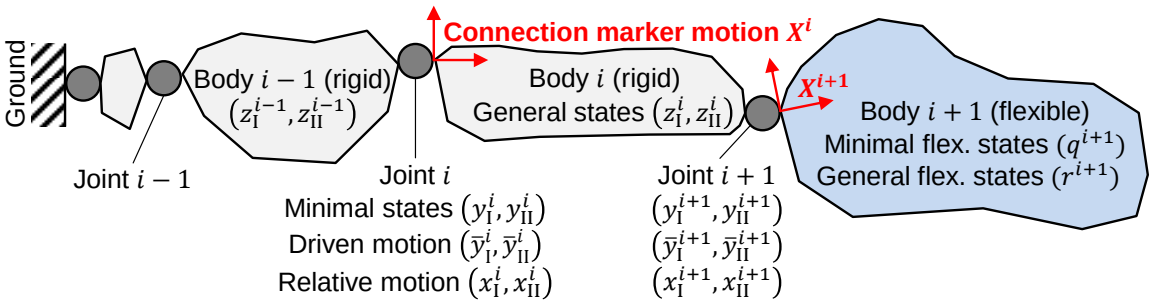

Figure 6 – Kinematic notation

where $\mathbf{M}$ denotes the mass matrix and h denotes the right hand side. For rigid bodies, the dynamic equation equals Newton's second law and z are the bodies' translatory and rotational velocities with respect to the inertial system $z = z_{\mathrm{II}}$. Depending on the kinematic configuration, there may be constraints $g(z) \equiv 0$ between the general states, resulting in a DAE for MBS dynamics. Accordingly, a constraint load term $\mathbf{G}^T \lambda$ appears in (6) with $\mathbf{G} = \frac{\partial g(z)}{\partial z}$ and the Lagrange multiplier λ. h is composed of gravity forces, centrifugal forces, gyroscopic moments as well as loads imprinted by internal and external force elements.

To satisfy the VAST model definition and the corresponding interface to the solver, the MBS dynamic equations must be provided in ODE form (see section 2.1). The latter requires a set of minimal states which are kinematically independent, and thus, not constrained by additional algebraic equations $g \equiv 0$. For rigid bodies, the joint states $(y_{\mathrm{I}}, y_{\mathrm{II}})$ are used as minimal states, based on the theory in [17]. Each joint degree of freedom (DoF) introduces one position level state in y_{I} (e. g. hinge angular deflection) and one velocity level state in y_{II} (e. g. hinge angular velocity). To satisfy the independence of the minimal states, only open loop MBS structures are allowed at the current stage of development. This means that each body is connected by exactly one joint to a preceding body or to the ground.

The development of ODE for the MBS bases on the joint kinematics. For each joint type, two kinematic functions are defined:

- The function
$$\dot{y}_{\mathrm{I}}^{i} = f(y_{\mathrm{I}}^{i}, y_{\mathrm{II}}^{i}) \tag{7}$$
returns the time derivative of the joint position states depending on the joint position and velocity states. For some (but not all!) joint types, it reduces to the trivial expression $\dot{y}_{\mathrm{I}}^{i} = y_{\mathrm{II}}^{i}$. The collection of this function from all joints in the MBS constitutes the first part (top rows) of the MBS ODE. This first part is called "kinematic ODE".

- The function
$$(x_{\mathrm{I}}^{i}, x_{\mathrm{II}}^{i}) = f(y_{\mathrm{I}}^{i}, y_{\mathrm{II}}^{i}, \bar{y}_{\mathrm{I}}^{i}, \bar{y}_{\mathrm{II}}^{i}) \tag{8}$$
returns the relative joint motion between the preceding and the current body. These are positions, rotations, translatory velocites and rotational velocites in all spatial directions. The relative kinematics $x_{\mathrm{I}}^{i}, x_{\mathrm{II}}^{i}$ may depend not only on the joint states, but also on driven motion $\bar{y}_{\mathrm{I}}^{i}, \bar{y}_{\mathrm{II}}^{i}$. For example, the rotor hub is often rotated with constant rotational speed relative to the fuselage by means of a driven hinge. In this case, the rotational speed and the corresponding rotational displacement are predefined, and thus, do not appear as states.

By looping through the MBS from the ground to the upper levels of the tree (fig. 6: from left to right), the general states $z_{\mathrm{I}}^{i}, z_{\mathrm{II}}^{i}$ of body i are obtained as

$$X^i = f(z_{\mathrm{I}}^{i-1}, z_{\mathrm{II}}^{i-1}, x_{\mathrm{I}}^{i}, x_{\mathrm{II}}^{i}), \tag{9}$$
$$(z_{\mathrm{I}}^{i}, z_{\mathrm{II}}^{i}) = f(X^i). \tag{10}$$

X^i is introduced for the sake of simplicity. It denotes the motion of body i's connection marker including translatory and rotational positions and velocities with respect to the inertial system. By using the

correlations (9) and (8), the general velocity states of the whole MBS can then be determined as $z_{\mathrm{II}} = f(y_{\mathrm{I}}, y_{\mathrm{II}}, \bar{y}_{\mathrm{I}}, \bar{y}_{\mathrm{II}})$. The application of the chain rule for $\dot{z}_{\mathrm{II}}$ yields

$$\dot{z}_{\mathrm{II}} = \underbrace{\frac{\partial z_{\mathrm{II}}}{\partial y_{\mathrm{II}}}}_{\mathbf{J}_y} \dot{y}_{\mathrm{II}} + \underbrace{\frac{\partial z_{\mathrm{II}}}{\partial y_{\mathrm{I}}} \dot{y}_{\mathrm{I}} + \frac{\partial z_{\mathrm{II}}}{\partial \bar{y}_{\mathrm{I}}} \dot{\bar{y}}_{\mathrm{I}} + \frac{\partial z_{\mathrm{II}}}{\partial \bar{y}_{\mathrm{II}}} \dot{\bar{y}}_{\mathrm{II}}}_{H}, \tag{11}$$

The Jacobians $\frac{\partial z_{\mathrm{II}}}{\partial y_{\mathrm{II}}}$, $\frac{\partial z_{\mathrm{II}}}{\partial y_{\mathrm{I}}}$, $\frac{\partial z_{\mathrm{II}}}{\partial \bar{y}_{\mathrm{I}}}$ and $\frac{\partial z_{\mathrm{II}}}{\partial \bar{y}_{\mathrm{II}}}$ are determined using automatic differentiation. Details on implementation are published in [18]. The insertion of (11) into (6) (note that $\dot{z} = \dot{z}_{\mathrm{II}}$ for rigid bodies) yields the MBS dynamic ODE in minimal coordinates y_{II}:

$$\mathbf{J}_y^T \mathbf{M} \mathbf{J}_y \dot{y}_{\mathrm{II}} = \mathbf{J}_y^T \left(h - \mathbf{M} H\right) \tag{12}$$

Due to $\mathbf{J}_y^T \mathbf{G}^T = 0$, the constraint load term has vanished in (12). The residual acceleration term H includes $\dot{y}_{\mathrm{I}}$ which is obtained from the previously evaluated kinematic ODE. The linear system of equations is solved utilizing QR-decomposition. Constraint forces and moments acting in the constrained joint directions (dimensions not included in (12)) are computed as a post-processing step, along with further MBS outputs such as the motion of markers defined on the bodies including acceleration terms as well as the potential and kinetic energy of the MBS.

4.2 Current Features and Verification

At the current stage of development, the VAST MBS model library provides the following types:

- Bodies: rigid body, flexible rod (prototype)
- Joints: Bracket (0 DoF), driven or freely moving slider (1 translatory DoF), driven or freely moving hinge (1 rotational DoF), free joint (6 DoF)
- Internal force elements
  - Rotational spring-damper elements around hinges
  - Translatory spring-damper elements between markers on different bodies
- External force elements
  - Arbitrarily configurable force elements
  - Airloads interface (automatic force element setup based on component configuration)

Since the implementation design of the MBS is modular, further types of bodies, joints and force elements may be added at any time. The systems that can be represented are limited to open-loop systems, i.e. a tree structure, where the branches do not reunite. However, an extension to closed loop-systems is planned for the near future.

To verify the MBS model an extensive cross-code verification campaign against the commercial MBS tool Simpack [3] has been conducted. From this campaign two simple example cases are shown here, a double pendulum and a test for gyroscopic effects. The double pendulum consists of two rigid bodies with mass and inertia each with a length of $2\,\mathrm{m}$ in their main direction. Both bodies have freely moving hinge joints as described above. The first body is connected to the ground and the second to the end of the first. At the second hinge, a rotational spring-damper element is acting dependent on the angular displacement and speed of the hinge. At the end of the second body an axial spring is placed exerting a force onto this point once the end leaves its starting point. During the simulation the double pendulum moves from its horizontal starting position under the influence of gravity. The resulting hinge angles are compared to the values computed with SIMPACK in fig. 7a. In all the figures of this section, the solid lines denote the reference values gathered with SIMPACK and the dashed lines are the VAST results. The match between SIMPACK and VAST results is exact up to numerical accuracy. This holds true also for the constraint forces, as an example the constraint forces in y direction at the joints are shown in fig. 7b.

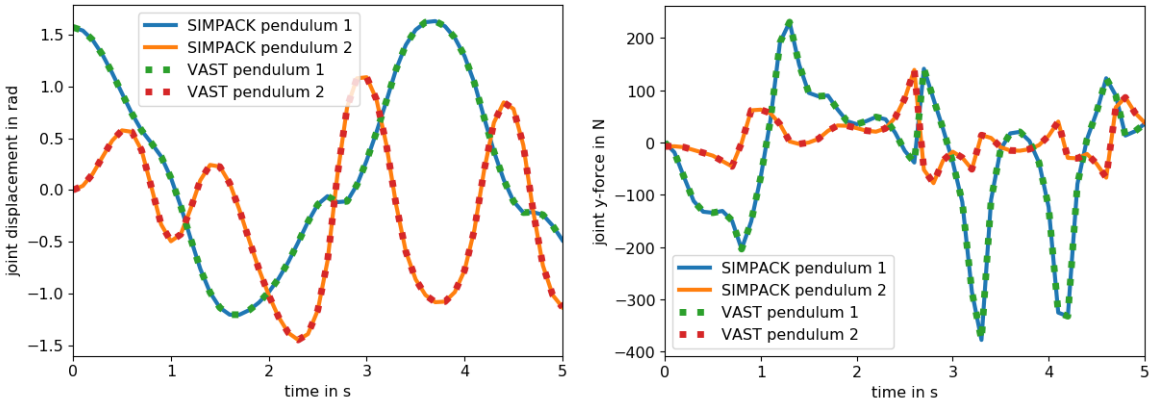

(a) Pendulum hinge angles over time

(b) Attachment y-force over time

Figure 7 – MBS test case: double pendulum, displacements and constraint forces in y

The second test case represents a rotating rotor blade that exhibits a flapping motion in vacuo. The flapping motion leads to a radial repositioning Δr of the center of gravity (CG) of the blade with respect to the rotor center (see fig. 8a showing the blade flapping upwards), which in turn creates a moment in the rotor-plane. This effect is known as Coriolis coupling and causes the blade to lead-lag. In the simulation only a hinge in flap direction is provided, so the coupling should be observed via a resulting constraint moment. At the beginning of the simulation, the blade is aligned horizontally and rotating around the vertical z-axis with a constant speed. Gravity induces the flapping motion of the blade. Fig. 8b shows the constraint torque in lead-lag direction. The perfect match of the VAST results with the SIMPACK calculations can be seen for this test case as well. A second gyroscopic effect that is verified by this test case is the centrifugal force that pushes the blade back towards the rotor plane.

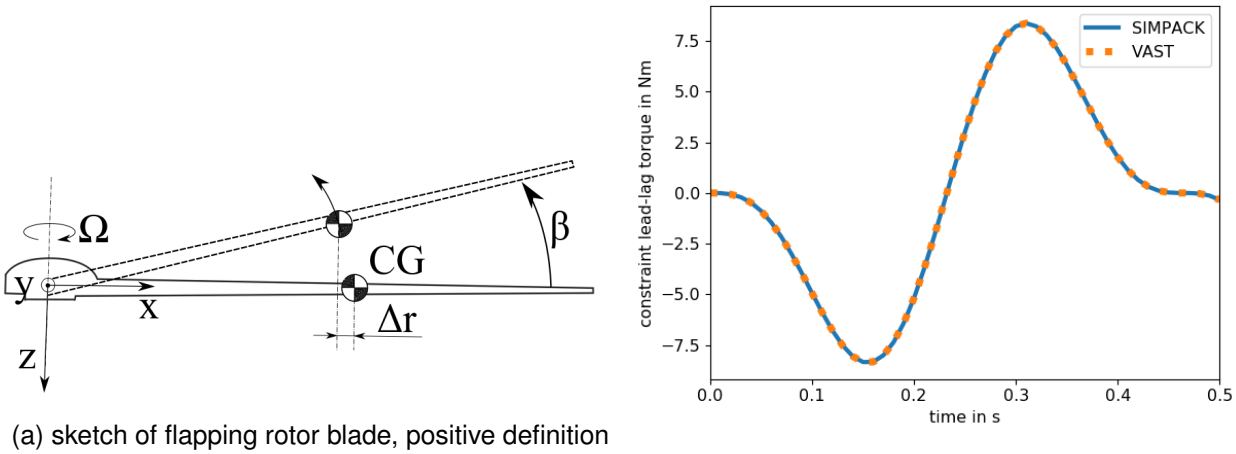

(a) sketch of flapping rotor blade, positive definition shown

(b) Coriolis moment at the rotor center

Figure 8 – MBS test case: Coriolis moment due to rotor blade flapping

5. Summary

A new simulation code for rotorcraft comprehensive analysis is being developed at the DLR. It uses a strictly generic approach of arbitrarily coupled state-space models, only being specific to helicopters in the available library of physical models. Even though some simulation tasks are implemented with features commonly needed for helicopters, no assumptions are made about the system to be simulated. This gives a lot of flexibility to the configuration of mechanical systems. Another advantage of this generic approach is that not only physical models or dynamic systems can be expressed as such a state-space model. Since the generic model interface allows also models with no states or no inputs, it is very flexible in what can be represented in a model still using the same base interface.

Pilot inputs or post-processing of specific outputs are only examples. This very generic approach makes VAST different from other helicopter simulation codes, which often distinguish structural, rotor, and aerodynamic models or kinematic and force coupling explicitly. This generality is a clear advantage over other comprehensive rotor codes, since it is well-maintainable, easy to extend with new models, and also able to not only simulate helicopters, but any other dynamical system, which can be expressed as a coupling of state-space models.
The currently implemented time-marching trim approach used in VAST allows to define arbitrary parameters to be tuned by the trim algorithm and arbitrary equations of the form (4) may be defined as trim objective. This general trim procedure does not make any additional assumptions about the dynamic systems. In contrast to other helicopter trim software, no periodicity of the solution is assumed, which makes it possible to trim much more complicated systems, for example, with a variable rotor speed. Again, this methodology is not specific to helicopters.
The two most important model groups for helicopter simulation have been discussed in this paper: aerodynamics and structure. At the current state of development rotors can be simulated using unsteady sectional airloads and a number of inflow models with varying complexity from Glauert to Freewake. These rotors can be combined to form arbitrary rotorcraft configurations, thanks to the MBS approach which can handle arbitrary open loop systems of rigid bodies.
All in all the VAST core and approach has already proven its potential as a valuable framework both for aircraft design as well as phenomenological research.

6. Outlook

Because of the generic coupling approach the description of a specific configuration is more complex than for an architecture tailored for this specific application. One of the next steps is to alleviate this fact with the concept of mechanical components. The rationale behind this is that mechanical systems of a certain family usually contain similar interfaces, e.g. a rotor always produces forces and moments via manipulation of the surrounding air. What in terms of physics models is needed, depends on the implementation and the desired level of fidelity. With this knowledge sets of configuration constraints can be developed, that greatly ease the configuration of commonly used system parts. Arbitrary systems can still be configured outside the component logic. Another area are derived component outputs. These are outputs which are not inherently created by one singular model and are only needed because a set of models describe a certain type of mechanical component. An example would be the thrust coefficient of a rotor. While the specialization in configuration can be done as a pre-processing step, many derived outputs have to be computed inside the simulation, since they are needed as inputs by other models.
The VAST trim performs well for typical flight conditions but being a time domain approach, it is limited to stable systems. It is also limited in its calculation speed since it depends on vanishing transients. In the future other trim procedures like frequency domain approaches may be implemented to expand the trim capabilities of VAST.
Validation against measurements especially for flight tests is still in the early phases. To ease this process a validation framework for VAST has been developed for the continuous integration system to support future development ensuring code integrity, correctness of its parts and an always up-to-date picture on the current predictive accuracy of the code. The continuous improvement of the latter is one of the main drivers for the development. Another is the area of applicability. The near future will see enhancements in structural modeling to flexible bodies and closed loop systems. The extension of analysis methods and many simpler flight mechanical models is another area.

References

[1] J. Hofmann and M. Röhrig-Zöllner. Coupling rotor dynamics with a parallel airflow simulation. In *ISC High Performance 2016 (ISC2016)*, 2016.

[2] D. A. Peters, D. D. Boyd, and C. J. He. A Finite-State Induced-Flow Model for Rotors in Hover and Forward Flight. *Journal of the American Helicoptesr Society*, Vol. 34,(4), October 1989.

[3] W. Rulka. SIMPACK - A Computer Program for Simulation of Large-motion Multibody Systems. In W. Schiehlen, editor, *Multibody Systems Handbook*. Springer, Berlin, Heidelberg, Germany, 1990.

[4] E. Hairer, C. Lubich, and M. Roche. *The Numerical Solution of Differential-Algebraic Systems by Runge-Kutta Methods*, volume 1409 of *Lecture Notes in Mathematics*. Springer, 1989.

[5] E. Kohlwey and M. Röhrig-Zöllner. Half-Explicit Exponential Runge–Kutta Methods for Index-1 DAEs in Helicopter Simulation. *Math. Comput. Sci.*, 13:341–365, 2019.

[6] D.A. Peters and D. Barwey. A general theory of rotorcraft trim. *Math. Probl. Eng.*, 2:1–34, 1996.

[7] J. Nocedal and S.J. Wright. *Numerical Optimization*. Springer, 2 edition, 2006.

[8] J. G. Leishman and T. S. Beddoes. A generalized model for airfoil unsteady aerodynamic behaviour and dynamic stall using the indicial method. In *42nd Annual Forum of the American Helicopter Society*, Washington D.C., June 1986.

[9] U. Leiss. A Consistent Mathematical Model to Simulate Steady and Unsteady Rotor-Blade Aerodynamics. In *10th European Rotorcraft Forum, The Hague, Netherlands*, 1984.

[10] M. Mindt. Merging an Analytical Aerodynamic Model for Helicopter Applications With a State-Space Formulation for Unsteady Airfoil Behavior. In *67. Deutscher Luft- und Raumfahrtkongress, Friedrichshafen, Germany*, September 4.-6., 2018.

[11] J. Rauleder, B. G. van der Wall, A. Abdelmoula, D. Komp, S. Kumar, V. Ondra, B. Titurus, and B. K. S. Woods. Aerodynamic performance of morphing blades and rotor systems. In *AHS International 74th Annual Forum and Technology Display*, Phoenix, Arizona, May 2018.

[12] H. Glauert. A General Theory of the Autogyro. Technical Report ARC R&M 1111, Aeronautical Research Council, 1926.

[13] D. M. Pitt and D. A. Peters. Theoretical Predictions of Dynamic Inflow Derivatives. *Vertica*, vol. 5, pp. 21–34, 1981.

[14] F. X. Caradonna and C. Tung. Experimental and Analytical Studies of a Model Helicopter Rotor in Hover. Technical Report NASA TM 81232, National Aeronautics and Space Administration, 1981.

[15] W. Schiehlen. Multibody System Dynamics:Roots and Perspectives. *Multibody System Dynamics*, 1(2):149–188, 1997.

[16] A. A. Shabana. Flexible Multibody Dynamics: Review of Past and Recent Developments. *Multibody System Dynamics*, 1(2):189–222, 1997.

[17] R. Schwertassek and O. Wallrapp. *Dynamik flexibler Mehrkörpersysteme: Methoden der Mechanik zum rechnergestützten Entwurf und zur Analyse mechatronischer Systeme*. Grundlagen und Fortschritte der Ingenieurwissenschaften. Vieweg, Braunschweig, 1999. ISBN: 978-3-528-06629-1.

[18] M. Kontak, M. Röhrig-Zöllner, J. Hofmann, and F. Weiß. Automatic Differentiation in Multibody Helicopter Simulation. In Andrés Kecskeméthy and Francisco Geu Flores, editors, *Multibody Dynamics 2019*, volume 53, pages 534–542. Springer International Publishing, Cham, 2020.

Copyright Statement